

Neural network parametrized level sets for image segmentation

Otmar Scherzer^{1,2,3}
 otmar.scherzer@univie.ac.at

Cong Shi^{1,2}
 cong.shi@univie.ac.at

Thi Lan Nhi Vu^{1,3}
 thi.lan.nhi.vu@univie.ac.at

¹Faculty of Mathematics
 University of Vienna
 Oskar-Morgenstern-Platz 1
 A-1090 Vienna, Austria

²Johann Radon Institute for Computational
 and Applied Mathematics (RICAM)
 Altenbergerstraße 69
 A-4040 Linz, Austria

³Christian Doppler Laboratory
 for Mathematical Modeling and Simulation
 of Next Generations of Ultrasound Devices (MaMSi)
 Oskar-Morgenstern-Platz 1
 A-1090 Vienna, Austria

Abstract

The Chan-Vese functionals have proven to be a first-class method for segmentation and classification. Previously they have been implemented with level-set methods based on a pixel-wise representation of the level-sets. Later parametrized level-set approximations, such as splines, have been studied. In this paper we consider neural networks as parametrized approximations of level-set functions. We show in particular, that parametrized two-layer networks are most efficient to approximate polyhedral segments and classes. We also prove the efficiency for segmentation and classification.

1. INTRODUCTION

Image segmentation and *classification* aims to partition an image into regions of desired properties. Accurate segmentation and classification plays a crucial role in many areas of applications such as object recognition, medical diagnosis, autonomous driving, and scene understanding, to name but a few.

Basis for this work are the variational Chan-Vese *segmentation* [4] and *classification* [14] methods. In these approaches, piecewise constant functions are computed that minimize an energy functional. The regions of constant intensity are the segments and classes to be detected. The theoretical foundations of the Chan-Vese model date back to the seminal work of Mumford & Shah [10] and Morel & Solimini [9]. In computational practice, the Chan-Vese functionals are often minimized via a level-set approach, where the segments and classes are represented by the level-sets. Level-set methods, originally introduced by Osher & Sethian [11], have proven a powerful approach to solve image segmentation and classification tasks, because the implicit representation of segments and classes allows to find objects of complex topologies, such as, for instance, segments consisting of multiple connected domains. There exist two categories of level-set algorithms (see Figure 1):

Unparametrized level-set algorithms consider the input images and the level-set functions, from which segments and classes are detected, pixel-wise. There, the data are represented as a vector of pixel values.

Parametrized algorithms (see, for instance, [15, 7, 2, 12]) use ansatz-functions (such as splines or finite elements) to represent the level-sets and input images. This means, in particular, that the segments and classes are specified *double implicitly*: as the zero level-sets of the representing functions (first), which in turn are represented via the parametrization (second).

The different concepts can be compared with *finite difference* and *finite element* methods for solving differential equations: The latter represents the solution of the differential equation implicitly by finite element parametrizations, whereas the former are given explicitly as function values on a grid. In fact, *hybrid* level-set algorithms combining the advantages of both parametrized and unparametrized strategies have also been developed (see [8]).

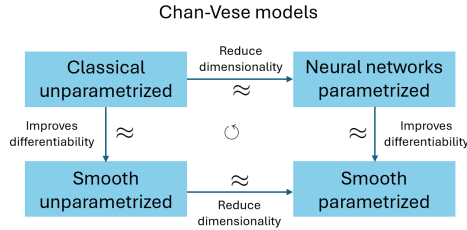


FIGURE 1. Commutative diagram illustrating the relationships among the classical, parametrized, and smooth Chan-Vese models. The classical (unparametrized) model can be approximated by the parametrized non-smooth model, which can then be approximated by the smooth variant.

The achievements of this paper are as follows:

- (i) We propose a *parametrized* Chan-Vese method for image segmentation and classification, where we use *deep neural networks* for parametrization of the level-set functions. The efficiency of neural networks is unquestioned nowadays, but there remains a lack of transparency regarding why this is the case and how they should be parametrized (that means, which networks one should implement)? Such a motivation is the first goal of this paper: We give illustrative examples that demonstrates why (deep) two-hidden-layer networks efficiently represent segments and classes (see Section 2) defined from level-sets. This result puts the mathematical foundations of level-set methods and neural networks in perspective (see Section 3).
- (ii) We use these insights to provide an efficient neural network parametrized Chan-Vese algorithm for segmentation and classification (see Section 4). We note that by classification, we mean determining which object a pixel in the image belongs to. This differs from the terminology commonly used in the machine learning community, where classification usually refers to assigning a category label to an entire image.

Before we go deeper into the analysis, we summarize the notations, which we use throughout the paper:

TABLE 1. Used notation

Name	Notation	Reference
Activation function	σ	(2.1)
Affine linear function	\mathbf{a}	(2.2)
Shallow neural network	\mathbf{s}	(2.3)
Deep neural network	\mathbf{t}	(2.5)
Set of one-layer networks	\mathbf{N}	(2.4)
Set of two-layer networks	\mathbf{T}	(2.6)
Number of neurons in the first layer	n_1	(2.3), (2.5)
Number of neurons in the second layer	n_2	(2.5)
Number of level lines	m	(3.1)
Multiphase level-set function	\mathbf{m}	(3.4)
A level-set function	ℓ	(3.5)
Regions to be segmented	Ξ_i	(3.5)
and their constant values	c_i	(3.7)
Unparametrized Chan-Vese functional	E_{CV}^f	(3.2), (3.6)
Parametrized Chan-Vese functional	E_{CV}^f	(3.9)

In the following, we start with an example motivating the efficiency of neural networks for segmentation. We then provide an overview of Chan-Vese segmentation models. Throughout this paper, we constrain ourselves to an image domain $\Omega \subseteq \mathbb{R}^2$, meaning that the application we have in mind is *image* segmentation

and classification. Without explicitly stating, we always assume that Ω is bounded, satisfies the cone property (see [1]), and has piecewise C^1 -boundary.

2. HEAVISIDE AND SIGMOID NETWORKS

In this section, we define Heaviside and sigmoid networks:

Definition 2.1 (Heaviside and sigmoid networks). Let $\varepsilon > 0$.

$$\sigma : \mathbb{R} \rightarrow \mathbb{R}, \quad x \mapsto \begin{cases} 1 & \text{for } x > 0 \\ \frac{1}{2} & \text{for } x = 0 \\ 0 & \text{for } x < 0 \end{cases} \quad \text{and} \quad \sigma_\varepsilon : \mathbb{R} \rightarrow \mathbb{R}, \quad x \mapsto \frac{1}{1 + e^{-\frac{x}{\varepsilon}}}, \quad (2.1)$$

are called Heaviside and sigmoid functions, respectively.

- A *Heaviside network function*, $N = \sigma \circ \mathbf{a}$, is a composition of an Heaviside and an *affine linear function*

$$\mathbf{a} : \mathbb{R}^2 \rightarrow \mathbb{R}, \quad \vec{x} \mapsto \vec{w}^T \vec{x} + b, \quad (2.2)$$

with parameters $\vec{w} \in \mathbb{R}^2, b \in \mathbb{R}$.

- A *one-layer (shallow) Heaviside network with n_1 neurons* (see Figure 2a) is a linear combination of Heaviside ansatz functions $N_j, j = 1, \dots, n_1$:

$$\vec{x} \in \mathbb{R}^2 \mapsto \mathbf{s}(\vec{x}) := \mathbf{s}[\vec{a}, \mathbf{W}, \vec{b}](\vec{x}) := \sum_{j=1}^{n_1} a_j N_j(\vec{x}) = \sum_{j=1}^{n_1} a_j (\sigma \circ \mathbf{a}_j)(\vec{x}) = \sum_{j=1}^{n_1} a_j \sigma(\vec{w}_j^T \vec{x} + b_j), \quad (2.3)$$

where $\mathbf{W} = (\vec{w}_1, \dots, \vec{w}_{n_1}) \in \mathbb{R}^{n_1 \times 2}$, $\vec{a} = (a_1, \dots, a_{n_1}) \in \mathbb{R}^{n_1}$ and $\vec{b} = (b_1, \dots, b_{n_1}) \in \mathbb{R}^{n_1}$ are called the parametrizations of the function \mathbf{s} . The set of all one-layer neural networks is denoted by

$$\mathbb{N} := \left\{ \mathbf{s}[\vec{a}, \mathbf{W}, \vec{b}] : \mathbf{W} \in \mathbb{R}^{n_1 \times 2}, \vec{a} \in \mathbb{R}^{n_1}, \vec{b} \in \mathbb{R}^{n_1} \right\}. \quad (2.4)$$

- A *two-layer Heaviside neural networks with n_1 neurons in the first layer and n_2 neurons in the second layer* (see Figure 2b) is defined as

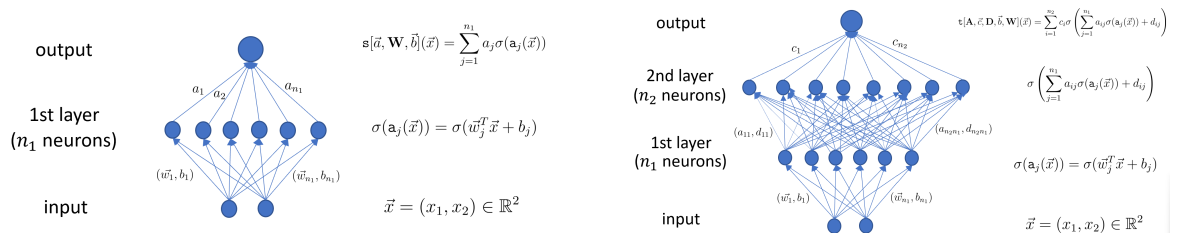
$$\vec{x} \in \mathbb{R}^2 \mapsto \mathbf{t}(\vec{x}) := \mathbf{t}[\mathbf{A}, \vec{c}, \mathbf{D}, \vec{b}, \mathbf{W}](\vec{x}) := \sum_{i=1}^{n_2} c_i \sigma \left(\sum_{j=1}^{n_1} a_{ij} \sigma(\mathbf{a}_j(\vec{x})) + d_{ij} \right). \quad (2.5)$$

$\mathbf{A} = (a_{ij}) \in \mathbb{R}^{n_2 \times n_1}$, $\vec{c} = (c_i) \in \mathbb{R}^{n_2}$, $\mathbf{D} = (d_{ij}) \in \mathbb{R}^{n_2 \times n_1}$ and $\vec{b} = (b_j) \in \mathbb{R}^{n_1}$, $\mathbf{W} = (w_{ij}) = (\vec{w}_j) \in \mathbb{R}^{n_1 \times 2}$ (note that \mathbf{a}_j depends on \mathbf{W} and \vec{b}) are the parametrization of \mathbf{t} . The set of all two-layer neural networks is denoted by

$$\mathbb{T} := \left\{ \mathbf{t}[\mathbf{A}, \vec{c}, \mathbf{D}, \vec{b}, \mathbf{W}] : \mathbf{A} \in \mathbb{R}^{n_2 \times n_1}, \vec{c} \in \mathbb{R}^{n_2}, \mathbf{D} \in \mathbb{R}^{n_2 \times n_1}, \vec{b} \in \mathbb{R}^{n_1}, \mathbf{W} \in \mathbb{R}^{n_1 \times 2} \right\}. \quad (2.6)$$

- A *sigmoid network* is defined analogously to a Heaviside network by replacing the Heaviside function σ with a sigmoid σ_ε . Accordingly, we denote one- and two-layer sigmoid network functions by $\mathbf{s}_\varepsilon, \mathbf{t}_\varepsilon$, respectively, and the set of one- and two-layer sigmoid networks by \mathbb{N}_ε and \mathbb{T}_ε , respectively.

We have schematically visualized the one- and two-layer networks in Figure 2.



(A) A one-layer neural network is used to approximate level-set (B) Two-layer deep neural network are used to approximate (multi)-phase functions.

FIGURE 2. One- and two-layer neural networks.

\mathbb{N} (see Equation 2.4) and \mathbb{T} (see Equation 2.6) are sets of neural networks. These sets are not minimal, meaning that different combinations of parameters can potentially represent a given function. Thus, in practice, the parameters are constrained, leading to customized networks:

Definition 2.2 (Customized two-layer network). The network

$$\mathbf{t}_c = \mathbf{t}_c[\vec{a}, \mathbf{W}, \vec{b}, d] : \mathbb{R}^2 \rightarrow \mathbb{R}, \quad \vec{x} \mapsto \sigma \left(\mathbf{s}[\vec{a}, \mathbf{W}, \vec{b}](\vec{x}) + d \right) = \sigma \left(\sum_{j=1}^{n_1} a_j \sigma(\vec{w}_j^T \vec{x} + b_j) + d \right), \quad (2.7)$$

is called a *customized* two-layer network (see Equation 2.5) with $n_2 = 1$, $c_1 = 1$ and $c_i = 0$ for $i > 1$, $a_{ij} = a_j$, and $d_{ij} = d$ for all i, j . The terms *customized* refers to the situation that several parameters are constant and not variable as in Equation 2.3 and Equation 2.5. In this customized architecture, the second layer consists of a single neuron. Although the network in Equation 2.7 is formally two-layered, only the first-layer parameters are trainable, while the second-layer parameters are fixed by construction. Thus, training reduces to a one-layer network Equation 2.3 followed by an activation.

2.1. Heaviside networks for parametrizations of polygons.

In the following, we consider the segmentation of a polygon in \mathbb{R}^2 , first illustrated with the example of a triangle (see Figure 3).

Example 2.3 (Heaviside network of a triangle). We consider three affine linear functions \mathbf{a}_j , $j = 1, 2, 3$, as defined in Equation 2.2 with $\vec{w}_j \neq 0$. In fact, the level-sets of these functions are straight lines. Associated with each function \mathbf{a}_j , $j = 1, 2, 3$, there are three sets

$$H_j^1 := \{\vec{x} : \mathbf{a}_j(\vec{x}) > 0\}, \quad H_j^0 := \{\vec{x} : \mathbf{a}_j(\vec{x}) = 0\} \quad \text{and} \quad H_j^{-1} := \{\vec{x} : \mathbf{a}_j(\vec{x}) < 0\}. \quad (2.8)$$

Assume that all 3 lines are in general position, meaning that no two lines are parallel and no three lines intersect at a single point, so that the combinatorial structure of the intersections is maximally generic. Then, there exist seven non-empty intersections of these sets, denoted by

$$\Omega_\iota := \bigcap_{j=1}^3 H_j^{\iota_j}, \quad \text{where } \iota = (\iota_1, \iota_2, \iota_3) \in \{-1, 1\}^3 \setminus \{(-1, -1, -1)\}.$$

Note that $\Omega_{(-1, -1, -1)} = \emptyset$ and is therefore not counted. Figure 3,2. visualizes the seven regions together with their associated triplets of values $(\sigma(\mathbf{a}_1), \sigma(\mathbf{a}_2), \sigma(\mathbf{a}_3))$.

Now we define a customized one-layer Heaviside neural network function (compare Equation 2.3), where the number of neurons equals the number of lines, that is, $n_1 = 3$:

$$\mathbf{s}_c(\vec{x}) := \sum_{j=1}^3 \frac{1}{3} \sigma(\mathbf{a}_j(\vec{x})) \quad \text{for all } \vec{x} \in \mathbb{R}^2. \quad (2.9)$$

In $\Omega \setminus (H_1^0 \cup H_2^0 \cup H_3^0)$, the function \mathbf{s}_c attains only three values $1/3, 2/3, 1$. Moreover, on each line H_j^0 , $j = 1, 2, 3$, the function $\mathbf{s}_c(\vec{x})$ can attain either the value $5/6, 1/2, 1/6$ depending on the configuration of the other two regions: either in $H_{j_1}^0 \cap (H_{j_2}^1 \cup H_{j_3}^1)$ or $H_{j_1}^0 \cap (H_{j_2}^{-1} \cup H_{j_3}^{-1})$, or in $H_{j_1}^0 \cap (H_{j_2}^{-1} \cup H_{j_3}^{-1})$ for every $j_1, j_2, j_3 = 1, 2, 3$, satisfying $j_1 \neq j_2 \neq j_3$. Therefore, for every κ satisfying $-1 < \kappa < -5/6$ (concretely, we choose $\kappa = -8/9$ below), a two-layer Heaviside network coincides with the characteristic function of the open triangle $\Omega_{1,1,1}$ is given by (compare with Equation 2.7)

$$\mathbf{t}_c^+(\vec{x}) = \sigma(\kappa + \mathbf{s}_c(\vec{x})) = \chi_{\Omega_{1,1,1}}(\vec{x}).$$

By adding the constant κ , we ensure that the value of \mathbf{t}_c^+ is zero outside $\Omega_{1,1,1}$, that is, whenever $\mathbf{s}_c(\vec{x}) \neq 1$. In particular, for all \vec{x} where $\mathbf{s}_c(\vec{x})$ attain the values $1/3, 2/3, 5/6, 1/2$, or $1/6$, choosing $-1 < \kappa < -5/6$ ensures that $\kappa + \mathbf{s}_c(\vec{x})$ is negative.

In a neural network analogy, $\sigma(\mathbf{a}_j)$, $j = 1, 2, 3$, corresponds to the activations of three neurons \mathbf{a}_j in the first layer. The functions \mathbf{s}_c and \mathbf{t}_c^+ denote customized one-layer and two-layer neural network, respectively. Some coefficients in the general form of a neural network have been customized, such as $a_j = 1/3$, for

$j = 1, 2, 3$, and $d = c$ fixed, for example $c = -8/9$, (see Equation 2.7). Conversely, the segmentation of the complementary region $\Omega \setminus \Omega_{1,1,1}$ is given by

$$\mathbf{t}_c^-(\vec{x}) := 1 - \sigma\left(-\frac{8}{9} + \mathbf{s}_c(\vec{x})\right) = \sigma\left(\frac{8}{9} - \mathbf{s}_c(\vec{x})\right) = \chi_{\Omega \setminus \Omega_{1,1,1}}(\vec{x}).$$

Therefore, we can define a piecewise constant function which attains two function values $c_{\pm 1}$:

$$\mathbf{t}(\vec{x}) = c_1 \mathbf{t}_c^+(\vec{x}) + c_{-1} \mathbf{t}_c^-(\vec{x}) = c_1 \chi_{\Omega_{1,1,1}}(\vec{x}) + c_{-1} \chi_{\Omega \setminus \Omega_{1,1,1}}(\vec{x}). \quad (2.10)$$

\mathbf{t} is a two-layer network (see Equation 2.5 and Equation 2.6) with coefficients

$$\mathbf{A} = (a_{ij}) \in \mathbb{R}^{2 \times 3}, a_{ij} = \frac{(-1)^{i-1}}{3} \text{ for all } j = 1, 2, 3, \quad \vec{c} = (c_1, c_{-1}) \in \mathbb{R}^2,$$

$$\mathbf{D} = (d_{ij}) \in \mathbb{R}^{2 \times 3}, d_{ij} = \frac{(-8)^i}{9} \text{ for all } j = 1, 2, 3, \quad \vec{b} \in \mathbb{R}^3, \quad \mathbf{W} \in \mathbb{R}^{3 \times 2}, \vec{w}_j \neq 0 \text{ for all } j = 1, 2, 3.$$

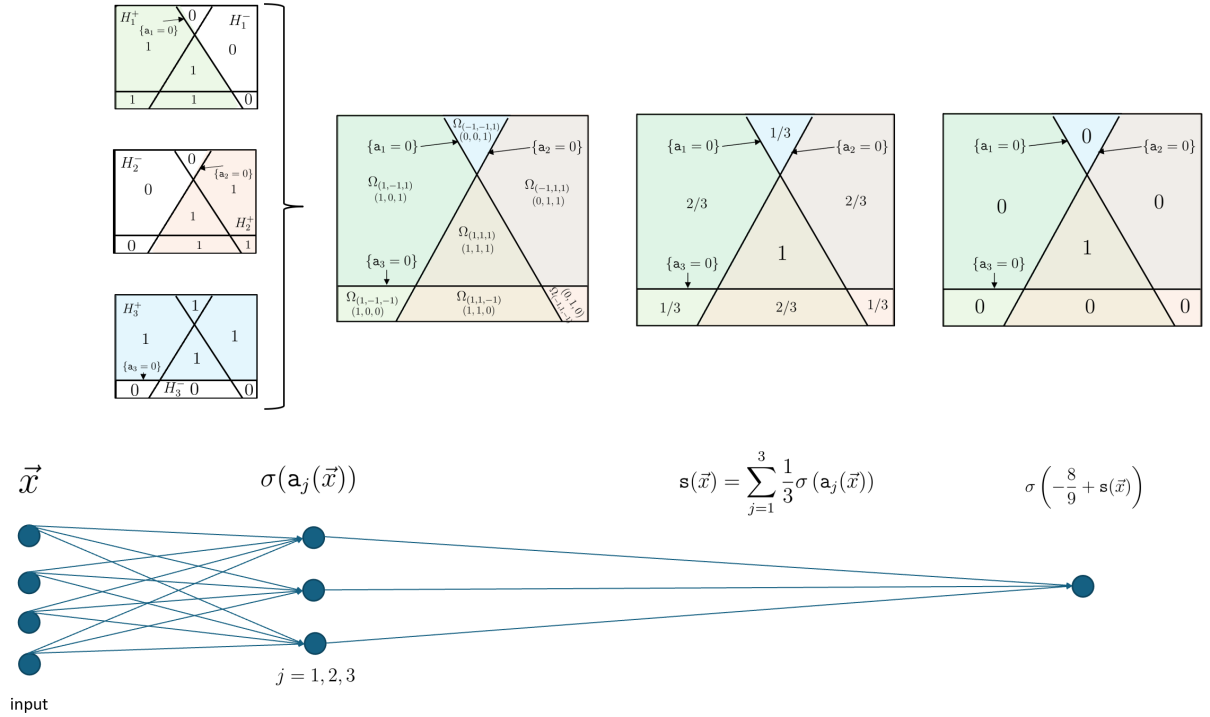


FIGURE 3. **1.** Each line $H_j^0 = \{\mathbf{a}_j = 0\}$, for $j = 1, 2, 3$, divides the image domain into 2 half-planes H_j^1 and H_j^{-1} . The half-planes containing the triangle T (shown in color) attain the value 1 and the complementary half-planes (left uncolored) attain 0. These 3 binary regions correspond to the activations of 3 neurons in the first layer of a neural network, represented by $\sigma(\mathbf{a}_j)$, $j = 1, 2, 3$, where $\mathbf{a}_j > 0$ inside the region and $\mathbf{a}_j(\vec{x}) < 0$ outside the region as the standard level-set method formulation.

2. Seven subregions Ω_i for $i \in (-1, 1)^3$ and their triplets of activation values $(\sigma(\mathbf{a}_1), \sigma(\mathbf{a}_2), \sigma(\mathbf{a}_3))$.

3. The average of these activations triplets are taken over each subregion Ω_i , resulting in values $1/3, 2/3, 1$. This corresponds to the linear combination $\mathbf{s}_c = \sum_{j=1}^3 \frac{1}{3} \sigma(\mathbf{a}_j)$.

4. Applying the activation $\sigma(-\frac{8}{9} + \mathbf{s}_c)$ to each subregion, only the region with $\mathbf{s}_c = 1$ outputs the value 1. This identifies the segmented regions $\Omega_{(1,1,1)} = T =: \Xi_1$. Conversely, applying the activation $-\sigma(-\frac{8}{9} + \mathbf{s}_c) + 1$ to each subregion yields the complementary regions $\Xi_{-1} = \Omega \setminus \Xi_1$.

This motivating example demonstrates the feasibility of using a customized two-layer neural network (see Equation 2.7) to represent the characteristic function of a convex polygon (see Lemma 2.4). Since polygons approximate arbitrary objects (see Figure 4), it can be anticipated that neural network level-sets are efficient parametrizations for level-set segmentation methods such as the Chan-Vese segmentation and classification methods, which are reviewed in the later sections.

Example 2.3 generalizes to any number of affine functions $n_1 \geq 3$. Generally, we have the following result:

Lemma 2.4. Let $n_1 \in \mathbb{N}, n_1 \geq 3$ be the number of affine linear functions \mathbf{a}_j with $\vec{w}_j \neq 0$ for $j = 1, \dots, n_1$, and let $\iota = (\iota_1, \dots, \iota_{n_1}) \in \{-1, 1\}^{n_1}$. Let $H_j^{\iota_j}$ be defined as in Equation 2.8. Assume that the lines H_j^0 are in general position. Then, there exist at most $\frac{n_1(n_1+1)}{2} + 1$ non-empty sets $\bigcap_{j=1}^{n_1} H_j^{\iota_j}$, and $\bigcap_{j=1}^{n_1} H_j^1$ is a n_1 -edges convex polygon.

Proof. The results can be proven by induction (see [13]). □

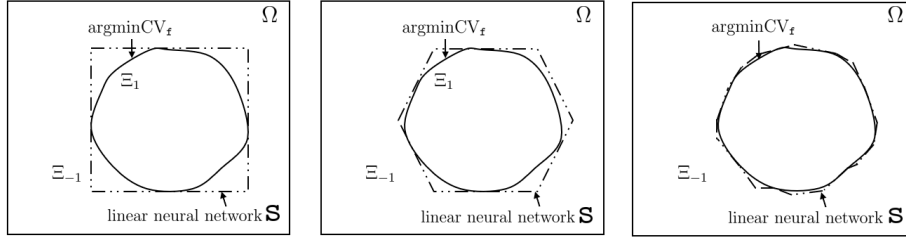


FIGURE 4. Polygonal approximation of arbitrary bounded regions. Increasing the number of polygonal edges, which corresponds to increasing the number of neurons n_1 in the network, improves the approximation accuracy.

3. CHAN-VESE SEGMENTATION AND CLASSIFICATION

We begin by reviewing the Chan–Vese segmentation and classification models (see [4, 14]), and the associated level-set method for computational implementation. In segmentation, a region is represented as the zero level-set of a function, whereas in classification, zeros of multiple level-set functions define classes (see Figure 5).

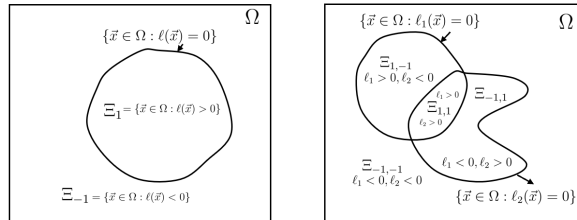


FIGURE 5. Image segmentation characterized by level-set functions and their signs. Here, 1 denotes the positive sign of a level-set function, corresponding to the inside of a region, and -1 denotes the negative sign, corresponding to the outside. **Left:** Segmentation with one level-set function ℓ ($m = 1$), Ω is segmented in two segments Ξ_1 and Ξ_{-1} . **Right:** Segmentation with two level-set functions ℓ_1, ℓ_2 ($m = 2$), Ω is segmented in four segments $\Xi_{\pm 1, \pm 1}$.

We present a unified formulation of Chan-Vese segmentation and classification: Let $m \in \mathbb{N}$ be given and let $\Omega \subseteq \mathbb{R}^2$, which is partitioned into at most 2^m subsets,

$$\{\Xi_\iota : \iota \in \{-1, 1\}^m\},$$

such that the intersection of any two subregions Ξ_ι either has positive Lebesgue measure or they are disjoint components, that is, for all $\iota \neq \iota'$ we have

$$\mu(\Xi_\iota \cap \Xi_{\iota'}) > 0 \quad \text{or} \quad \Xi_\iota \cap \Xi_{\iota'} = \emptyset.$$

Figure 6 illustrates the possible types of intersections between two subregions.

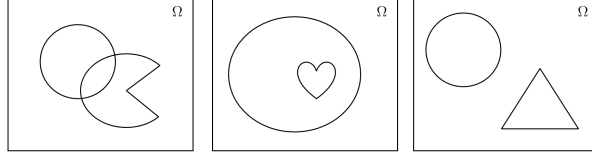


FIGURE 6. Different types of intersections of two subregions Ξ_i and $\Xi_{i'}$. **Left:** The intersection has positive Lebesgue measure, but neither region is contained in the other, i.e., $mu(\Xi_i \cap \Xi_{i'}) > 0, \Xi_i \Delta \Xi_{i'} \neq \emptyset$. **Middle:** One region is contained within the other, $\Xi_i \subseteq \Xi_{i'}$. **Right:** The two regions are disjoint, $\Xi_i \cap \Xi_{i'} = \emptyset$.

When $m = 1$, the index set of i is simply the set $\{-1, 1\}$ and Ξ_1 corresponds to a segment and Ξ_{-1} corresponds to the region outside the segment. Analogously, when $m = 2$, the index set of i contains four elements $\{(1, 1), (1, -1), (-1, 1), (-1, -1)\}$, which represent four different classes.

The Chan-Vese model is designed to approximate a given function $\mathbf{f} : \Omega \rightarrow \mathbb{R}$ by a multiphase function

$$\mathbf{m}(\vec{x}) = \sum_{i \in \{-1, 1\}^m} c_i \chi_{\Xi_i}(\vec{x}). \quad (3.1)$$

This is achieved by minimizing the Chan-Vese functional

$$CV_{\mathbf{f}}(\{(c_i, \Xi_i)\}_{i \in \{-1, 1\}^m}) = \sum_{i \in \{-1, 1\}^m} \int_{\Xi_i} (\mathbf{m} - \mathbf{f})^2 d\vec{x} + \mu \sum_{i \in \{-1, 1\}^m} \mathcal{H}^1(\partial \Xi_i) + \nu \mathcal{H}^2 \left(\bigcup_{i \in \{-1, 1\}^m} \Xi_i \right). \quad (3.2)$$

Remark 3.1. Since the one-dimensional measures of all $\partial \Xi_i$ are penalized, each Ξ_i must be a set of finite perimeter (a Caccioppoli set), meaning that $\partial \Xi_i$ is measurable with finite one-dimensional measure. Moreover, the main theorem of [9, Chapter 5] guarantees the existence of a segmentation $K := \{\partial \Xi_i\}_{i \in \{-1, 1\}^m}$ that minimizes the functional $CV_{\mathbf{f}}$. The minimizer is not unique (see [9, Chapter 15]). Furthermore, the theorem states that each $\partial \Xi_i$ of this minimizer is either a regular C^1 curve, or a piecewise regular C^1 curve with singular points consisting of triple junctions, where three branches meet at 120° angles, or boundary points where K meets $\partial \Omega$ at 90° angles. This suggests that the problem can be studied within a (piecewise) C^1 framework, which is convenient for variational approximation results such as Γ -convergence, ensuring the convergence of minimizers of approximate energies used in numerical applications (see Remark 3.8).

3.1. Numerical minimization of the Chan-Vese functional.

Chan & Vese [4, 14] proposed a level-set formulation of the functional defined in Equation 3.2 to minimize it numerically. The formulation utilizes that a piecewise constant function \mathbf{m} can be represented as a *multiphase level-set function* (see Equation 2.10):

Definition 3.2 (Multiphase level-set function). Let $m \in \mathbb{N}$ (see the example of triangle Example 2.3).

For every $k = 1, \dots, m$, let $\ell_k \in C^0(\bar{\Omega})$ be a *level-set function*, which means that it satisfies

$$\begin{aligned} H_k^1 &= \{\vec{x} \in \Omega : \ell_k(\vec{x}) > 0\} \text{ with } \mathcal{H}^2(H_k^1) < \infty \text{ and} \\ H_k^{-1} &= \{\vec{x} \in \Omega : \ell_k(\vec{x}) < 0\} \text{ and} \\ \partial H_k^1 &= \{\vec{x} \in \Omega : \ell_k(\vec{x}) = 0\} \text{ with } \mathcal{H}^1(\partial H_k^1) < \infty. \end{aligned} \quad (3.3)$$

$H_k^{\pm 1}$ represents two classes. In the language of level-set methods, Equation 3.3 means that the 0-level-set is not fat. We emphasize that a distance function of a domain is a typical example of a level-set function.

A *multiphase level-set function of degree 2^m* is a $L^2(\Omega)$ function of the form

$$\mathbf{m}(\vec{x}) = \sum_{i=(i_1, \dots, i_m) \in \{-1, 1\}^m} c_i \prod_{k=1}^m \sigma(i_k \ell_k(\vec{x})). \quad (3.4)$$

We use the same notation as in [Example 2.3](#), but note that here, the level-set function ℓ is an arbitrary function, while in [Example 2.3](#) the level-set function is \mathbf{a} , which is affine linear. Since we assumed that Ω is bounded, $\mathbf{m} \in L^2(\Omega)$ is piecewise constant and attains values $c_i \in \mathbb{R}$ on the interior of at most 2^m regions S_i , $i \in \{-1, 1\}^m$, respectively. That is,

$$\mathbf{m}(\vec{x}) = \sum_{i \in \{-1, 1\}^m} c_i \chi_{S_i}(\vec{x}) \text{ for almost all } \vec{x} \in \Omega,$$

where

$$S_i = \bigcap_{k=1}^m \{\vec{x} \in \Omega : \iota_k \ell_k(\vec{x}) > 0\}, \quad \bigcup_{i \in \{-1, 1\}^m} \partial S_i = \bigcup_{k=1}^m \{\vec{x} \in \Omega : \ell_k(\vec{x}) = 0\}. \quad (3.5)$$

Remark 3.3. According to [Definition 3.2](#), if we aim to identify s classes, we need at least $\lceil \log_2 s \rceil$ level-set functions, where $\lceil \cdot \rceil$ denotes the smallest integer greater than or equal to its argument.

The Chan-Vese functional, defined in [Equation 3.2](#), for minimizing piecewise constant functions \mathbf{m} , can be reformulated in terms of multiphase level-set functions (see [Definition 3.2](#)) as follows

$$\begin{aligned} & \text{CV}_{\mathbf{f}}^{\text{LS}}((c_i)_{i \in \{-1, 1\}^m}, (\ell_k)_{k=1}^m) \\ &:= \sum_{i \in \{-1, 1\}^m} \int_{\Omega} (c_i - \mathbf{f}(\vec{x}))^2 \prod_{k=1}^m \sigma(\iota_k \ell_k(\vec{x})) \, d\vec{x} \\ & \quad + \mu \sum_{k=1}^m \mathcal{H}^1(\{\ell_k = 0\}) + \nu \mathcal{H}^2\left(\bigcup_{j=1}^m \{\ell_j > 0\}\right) \\ &= \sum_{i \in \{-1, 1\}^m} \int_{\Omega} (c_i - \mathbf{f}(\vec{x}))^2 \prod_{k=1}^m \sigma(\iota_k \ell_k(\vec{x})) \, d\vec{x} \\ & \quad + \mu \sum_{k=1}^m \int_{\Omega} \delta(\ell_k(\vec{x})) |\nabla \ell_k(\vec{x})| \, d\vec{x} + \nu \left(\sum_{k=1}^m (-1)^{k+1} \sum_{\substack{A \subseteq \{1, 2, \dots, m\} \\ |A|=k}} \int_{\Omega} \prod_{k \in A} \sigma(\ell_k(\vec{x})) \, d\vec{x} \right). \end{aligned} \quad (3.6)$$

Note that the length term $\delta(\ell_k) |\nabla \ell_k|$ is understood in a distributional sense: it defines a one-dimensional measure supported on the zero level-set of ℓ_k , integrating along the normal direction to the curve. Here, the one-dimensional Dirac mass δ is the distributional derivative of the Heaviside function σ .

Example 3.4. For $m = 1$ and $m = 2$, the Chan-Vese functional looks as follows:

(i) $m = 1$:

$$\begin{aligned} \text{CV}_{\mathbf{f}}^{\text{LS}}(c_1, c_{-1}, \ell) &= \int_{\Omega} (\mathbf{f}(\vec{x}) - c_1)^2 \sigma(\ell(\vec{x})) \, d\vec{x} + \int_{\Omega} (\mathbf{f}(\vec{x}) - c_{-1})^2 (1 - \sigma(\ell(\vec{x}))) \, d\vec{x} \\ & \quad + \mu \int_{\Omega} \delta(\ell) |\nabla \ell| \, d\vec{x} + \nu \int_{\Omega} \sigma(\ell(\vec{x})) \, d\vec{x}. \end{aligned}$$

This is used for segmentation applications. In practice, the coefficients are customized to $c_1 = 1$ and $c_{-1} = -1$.

(ii) $m = 2$:

$$\begin{aligned} & \text{CV}_{\mathbf{f}}^{\text{LS}}((c_i), \ell_1, \ell_2) \\ &= \int_{\Omega} (\mathbf{f}(\vec{x}) - c_{1,1})^2 \sigma(\ell_1(\vec{x})) \sigma(\ell_2(\vec{x})) \, d\vec{x} + \int_{\Omega} (\mathbf{f}(\vec{x}) - c_{1,-1})^2 \sigma(\ell_1(\vec{x})) (1 - \sigma(\ell_2(\vec{x}))) \, d\vec{x} \\ & \quad + \int_{\Omega} (\mathbf{f}(\vec{x}) - c_{-1,1})^2 (1 - \sigma(\ell_1(\vec{x}))) \sigma(\ell_2(\vec{x})) \, d\vec{x} + \int_{\Omega} (\mathbf{f}(\vec{x}) - c_{-1,-1})^2 (1 - \sigma(\ell_1(\vec{x}))) (1 - \sigma(\ell_2(\vec{x}))) \, d\vec{x} \\ & \quad + \mu \int_{\Omega} \delta(\ell_1) |\nabla \ell_1| + \delta(\ell_2) |\nabla \ell_2| \, d\vec{x} + \nu \int_{\Omega} \sigma(\ell_1(\vec{x})) + \sigma(\ell_2(\vec{x})) - \sigma(\ell_1(\vec{x})) \sigma(\ell_2(\vec{x})) \, d\vec{x}. \end{aligned}$$

Note that we have $\sigma(-x) = 1 - \sigma(x)$ for all $x \in \mathbb{R}$, therefore $(1 - \sigma(\ell_i)) = \sigma(-\ell_i)$ for $i = 1, 2$.

Vese & Chan [14] suggested an evolution process, in which $(\ell_k(t, \vec{x}))_{k=1}^m$ and $(c_i(t))_{i \in \{-1,1\}^m}$ evolve with time t and, as $t \rightarrow \infty$, approximate the minimizers $(\ell_k)_{k=1}^m$ of $\text{CV}_{\mathbf{f}}^{\text{LS}}$ defined in Equation 3.6 and the corresponding constants $(c_i)_{i \in \{-1,1\}^m}$. Concretely, starting from some initial level-sets $\{\ell_{k,0} = 0 : k = 1, \dots, m\}$ and from the initial constant values $c_i(0)$ on the level-sets, satisfying,

$$\ell_k(0, \vec{x}) = \ell_{k,0}(\vec{x}) \text{ for } \vec{x} \in \Omega \text{ and } c_i(0) = \frac{\int_{\Omega} \mathbf{f}(\vec{x}) \prod_{k=1}^m \sigma(\nu_k \ell_{k,0}(\vec{x})) d\vec{x}}{\int_{\Omega} \prod_{k=1}^m \sigma(\nu_k \ell_{k,0}(\vec{x})) d\vec{x}},$$

the evolution process is governed by the system

$$\left\{ \begin{array}{l} \frac{\partial \ell_k}{\partial t}(t, \vec{x}) = \delta(\ell_k)(t, \vec{x}) \left[\mu \operatorname{div} \left(\frac{\nabla \ell_k}{|\nabla \ell_k|} \right) (t, \vec{x}) \right. \\ \quad - \nu \sum_{j=1}^m (-1)^{j+1} \sum_{\substack{A \subseteq \{1,2,\dots,m\} \\ |A|=j}} \prod_{\substack{i \in A \\ i \neq j}} \sigma(\ell_i)(t, \vec{x}) \\ \quad \left. - \sum_{i \in \{-1,1\}^m} \nu_i (c_i(t) - \mathbf{f}(\vec{x}))^2 \right] \text{ for } (t, \vec{x}) \in (0, \infty) \times \Omega, \\ \text{together with boundary conditions} \\ \frac{\delta(\ell_k)(t, \vec{x})}{|\nabla \ell_k(t, \vec{x})|} \frac{\partial \ell_k}{\partial \vec{n}}(t, \vec{x}) = 0 \text{ for } (t, \vec{x}) \in (0, \infty) \times \partial \Omega, \\ \text{and the evolution for } c_i : \\ c_i(t) = \frac{\int_{\Omega} \mathbf{f}(\vec{x}) \prod_{k=1}^m \sigma(\nu_k \ell_k(t, \vec{x})) d\vec{x}}{\int_{\Omega} \prod_{k=1}^m \sigma(\nu_k \ell_k(t, \vec{x})) d\vec{x}} \text{ for } t \in (0, \infty). \end{array} \right. \quad (3.7)$$

Here, each ℓ_k , $k = 1, \dots, m$, evolves in the direction normal to its level-lines.

In contrast to the standard pixel-based formulation (unparametrized) of the Chan-Vese functional, see Equation 3.6, we consider now a *parametrized* Chan-Vese model, where neural networks are used to represent the piecewise constant segmentation functions \mathbf{m} .

3.2. Neural networks parametrized Vese-Chan classification.

We consider the Vese-Chan classification, where the level-set functions $\{\ell_k : k = 1, \dots, m\}$ (see Equation 3.4) are approximated by one-layer Heaviside networks:

$$\vec{x} \in \Omega \subseteq \mathbb{R}^2 \mapsto \mathbf{m}_{\mathbf{s}}(\vec{x}) := \sum_{i \in \{-1,1\}^m} c_i \prod_{k=1}^m \sigma(\nu_k \mathbf{s}_k(\vec{x})). \quad (3.8)$$

In comparison with Equation 3.4, we now have σ composed with \mathbf{s}_k instead of ℓ_k , where

$$\mathbf{s}_k := \mathbf{s}[\vec{a}_k, \mathbf{W}_k, \vec{b}_k] := \sum_{j=1}^{n_1} (\vec{a}_k)_j \sigma((\mathbf{W}_k)_j^T \vec{x} + (\vec{b}_k)_j)$$

is defined in Equation 2.3 with $(\vec{a}_k)_j, (\vec{b}_k)_j \in \mathbb{R}$ denoting the j -th elements of the vectors $\vec{a}_k, \vec{b}_k \in \mathbb{R}^{n_1}$, respectively, and $(\mathbf{W}_k)_j \in \mathbb{R}^2$ is the j -th column of the matrix $\mathbf{W}_k \in \mathbb{R}^{n_1 \times 2}$.

In this case, the corresponding regions S_l formed by $\mathbf{m}_{\mathbf{s}}$, as defined in Equation 3.3, are polygonal sets. Hence, we denote them by P_l :

$$\mathbf{m}_{\mathbf{s}} = \sum_{i \in \{-1,1\}^m} c_i \chi_{P_i}(\vec{x}).$$

Definition 3.5. The one-layer network parametrized Chan-Vese functional is defined by

$$\begin{aligned} \text{CV}_{\mathbf{f}}^{\text{LS}}((c_i)_{i \in \{-1,1\}^m}, (\vec{a}_k, \mathbf{W}_k, \vec{b}_k)_{k=1}^m) &= \sum_{i \in \{-1,1\}^m} \int_{\Omega} (c_i - \mathbf{f}(\vec{x}))^2 \prod_{k=1}^m \sigma(\nu_k \mathbf{s}_k(\vec{x})) d\vec{x} \\ &+ \mu \sum_{k=1}^m \mathcal{H}^1(\{\mathbf{s}_k = 0\}) + \nu \mathcal{H}^2 \left(\bigcup_{k=1}^m \{\mathbf{s}_k > 0\} \right). \end{aligned} \quad (3.9)$$

The one-layer network parametrized Chan-Vese functional can be used for classification and segmentation: Instead of finding arbitrary level-set functions, which determine the classes of the function \mathbf{f} , by minimizing $\text{CV}_{\mathbf{f}}^{\text{LS}}$ from Equation 3.6, we constrain the optimization of the functional to polyhedral classes.

We recall that the maximum number of objects to be segmented or classified is 2^m . The numbers of neurons $n_1 \in \mathbb{N}$ corresponds to the number of polygonal edges in the polygonal approximation of a single object: larger values of n_1 yield more accurate approximations (see Example 2.3). Although n_1 can vary between objects, for notational simplicity we assume, that all objects are approximated by polygons with the same number of edges n_1 .

Moreover, the function \mathbf{m}_s from Equation 3.8 coincides pointwise with a two-layer Heaviside network \mathbf{t}_m as defined in Equation 2.5:

Lemma 3.6. *Let $m \in \mathbb{N}$ be fixed. Then, every \mathbf{m}_s from Equation 3.8 can be represented as*

$$\mathbf{t}_m(\vec{x}) = \sum_{\iota \in \{-1,1\}^m} c_\iota \chi_{P_\iota}(\vec{x}) = \sum_{\iota \in \{-1,1\}^m} c_\iota \sigma \left(\kappa + \sum_{j=1}^m \sigma(\iota_j \mathbf{a}_j(\vec{x})) \right) \in \mathbb{T}, \quad (3.10)$$

for a fixed constant $\kappa \in \mathbb{R}$ satisfying $-m < \kappa < -m + 1/2$.

The proof follows from the fact that each term $\sigma(\iota_j \mathbf{a}_j(\vec{x}))$ takes values in $\{0, 1/2, 1\}$, and therefore, the sum $\sum_{j=1}^m \sigma(\iota_j \mathbf{a}_j(\vec{x}))$ takes values in $\{0, 1/2, 1, 3/2, \dots, m\}$. If all terms equal 1, then the sum equals m . Otherwise, the maximal possible value is $m - 1/2$. As a result, for constants κ satisfying $-m < \kappa < -m + 1/2$, the expression $\sum_{j=1}^m \sigma(\iota_j \mathbf{a}_j(\vec{x})) + \kappa$ is positive if and only if $\sigma(\iota_j \mathbf{a}_j(\vec{x})) = 1$ for all $j = 1, \dots, m$, which means that

$$\chi_{S_\iota}(\vec{x}) = \sigma \left(\sum_{j=1}^m \sigma(\iota_j \mathbf{a}_j(\vec{x})) + \kappa \right) = \mathbf{t}_c \in \mathbb{T} \quad (3.11)$$

pointwise in Ω . For concreteness, we can choose $\kappa = -m + 1/3$.

Equation 3.10 shows that the multiphase piecewise-constant Chan-Vese classification model (Equation 3.4) can be approximated by two-layer Heaviside networks as defined in Equation 2.5. We note that \mathbf{t}_m is a weakly customized network with some fixed parameters ($a_{ij} = 1$, $d_{ij} = \kappa$). Moreover, Equation 3.11 corresponds to a heavily customized two-layer network \mathbf{t}_c as defined in Equation 2.7, which by construction is equivalent to a one-layer network followed by a single Heaviside activation.

Together, these findings establish a structural link between the Chan-Vese model and neural networks (see Figure 7). In particular, the classical level-set formulation can be expressed in a neural-network approximation, facilitating numerical implementation using established architectures and optimization algorithms. The analysis also identifies that a minimal depth of two layers is sufficient for image segmentation and classification.

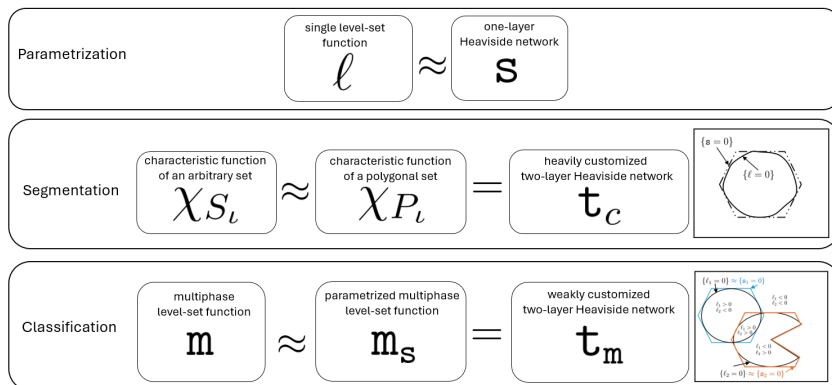


FIGURE 7. The Chan-Vese segmentation corresponds to the zero level set of a function that can be approximated by a one-layer Heaviside network (Equation 2.3). The characteristic function of the segmented region can be approximated by a heavily customized two-layer Heaviside network \mathbf{t}_c (Equation 2.7), while the multiphase piecewise-constant Chan-Vese classification function \mathbf{m} (Equation 3.4) can be approximated by a weakly customized two-layer Heaviside network \mathbf{t}_m (Equation 3.10).

3.3. Regularized Heaviside networks.

For numerical implementation, the Heaviside function in the parametrized Chan-Vese functional $\text{CV}_{\mathbf{f}}^{\text{LS}}$ (see Equation 3.8) is approximated by a sigmoid function σ_{ε} . With this approximation, we obtain the functional $\text{CV}_{\mathbf{f},\varepsilon}^{\text{LS}}$. Accordingly, if we use σ_{ε} instead of σ in the definition of one-layer networks \mathbf{s} in \mathbb{N} (see Equation 2.3) and \mathbf{t} in \mathbb{T} (see Equation 2.5), we get respectively \mathbf{s}_{ε} in \mathbb{N}_{ε} and \mathbf{t}_{ε} in \mathbb{T}_{ε} . In the following, we justify the approximation σ_{ε} of σ by the following lemma:

Lemma 3.7 (Properties of σ_{ε}). *For all $\varepsilon > 0$, the sigmoid function σ_{ε} is Lipschitz continuous, and the family $\{\sigma_{\varepsilon} : \varepsilon > 0\}$ approximates the Heaviside function σ in $L^1(\mathbb{R})$, $L^2(\mathbb{R})$, and pointwise in \mathbb{R} .*

Remark 3.8 (Γ -convergence under certain regularity assumptions). We can expect that minimizing the Chan-Vese functional $\text{CV}_{\mathbf{f}}(\{(c_i, \Xi_i)\}_{i \in \{-1,1\}^m})$ (see Equation 3.2) and the Chan-Vese level-set functional Equation 3.6 provide the same minimizers under certain regularity assumptions on the classes to be identified. Then the results of [9] for Equation 3.2 (cf. Remark 3.1) carry over to the minimizers of Equation 3.6: Indeed, if each boundary $\partial\Xi_i$, which is a segment of the function \mathbf{f} , is a regular C^1 curve, then it is a one-dimensional C^1 embedded manifold. Hence, there exist a C^1 function whose zero level-set coincides with $\partial\Xi_i$. Conversely, given a C^1 function whose zero level-set is regular, this set is a one-dimensional manifold and can be parametrized by finite number of closed regular C^1 curves. Under these regularity assumptions, the regularized Chan-Vese functional $\text{CV}_{\mathbf{f},\varepsilon}^{\text{LS}}$ (i.e., the functional $\text{CV}_{\mathbf{f}}^{\text{LS}}$ in Equation 3.6 with sigmoid σ_{ε} replacing Heaviside σ) Γ -converges (see for instance [5]) to the functional $\text{CV}_{\mathbf{f}}^{\text{LS}}$. If, for each level-set function ℓ_k in C^1 , there exists an one-layer sigmoid network $\mathbf{s}_{k,\varepsilon} := \mathbf{s}_{\varepsilon}[\vec{a}_k, \mathbf{W}_k, \vec{b}_k] \in \mathbb{N}_{\varepsilon}$ that approximates ℓ_k in C^1 , and for each $\varepsilon > 0$, the functional $\text{CV}_{\mathbf{f},\varepsilon}^{\text{LS}}$ attains a minimizer $(c_i^{\varepsilon}, \ell_{k,\varepsilon}) \in \mathbb{R} \times C^1(\bar{\Omega})$, then, there exists a sequence of one-layer sigmoid networks $(\mathbf{s}_{k,\varepsilon})_{\varepsilon} \subseteq \mathbb{N}_{\varepsilon}$ such that a subsequence, together with the corresponding constant c_i^{ε} , converges to a minimizer $(c_i, \ell_k) \in \mathbb{R} \times C^1(\bar{\Omega})$ of the functional $\text{CV}_{\mathbf{f}}^{\text{LS}}$, if exists.

3.4. Algorithm.

In order to minimize the one-layer parametrized Chan-Vese functional, defined in Equation 3.9, which is highly non-convex with respect to the parameters (c_i) , $(\vec{a}_k, \mathbf{W}_k, \vec{b}_k)_{k=1}^m$ an appropriate initialization of the network parameters is required. This initialization is obtained through a learning process, which is based on two main steps:

- **Step 1:** Train a neural network to generate an initial network structure for parametrization (c_i) , $(\vec{a}_k, \mathbf{W}_k, \vec{b}_k)_{k=1}^m$ (algorithm 1). The basic learning framework is summarized in Figure 8. The training, validation and testing procedure is summarized in algorithm 1.
- **Step 2:** After training, the optimized network parameters initialize the evolution of the level-set functions, which is driven by stochastic optimization of the network parameters to minimize the parametrized Chan-Vese functional $\text{CV}_{\mathbf{f},\varepsilon}^{\text{LS}}$ (see algorithm 2).

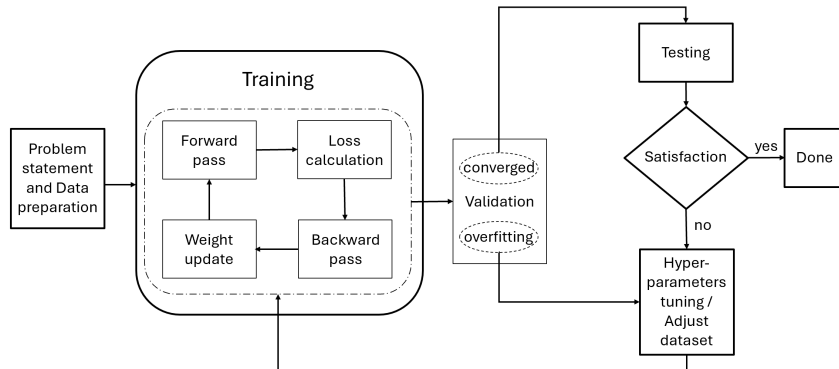


FIGURE 8. Flowchart of the prior learning process.

Algorithm 1: Training 1-Layer Neural Network for Multiphase Segmentation

Input: Training set $\mathcal{F} = \{\mathbf{f}_{\text{input}}^i\}$, (Optional) Targeted set $\mathcal{T} = \{\mathbf{f}_{\text{target}}^i\}$, Validation set $\mathcal{G} = \{\mathbf{g}^i\}$,
 m phases, n_1 neurons, max epochs E , patience P , (Optional) Supervised loss \mathcal{L} , Optimizer

Output: Trained parameters $\tilde{\Theta}$

```

// Initialize m networks
for k = 1 to m do
     $\vec{a}_k \in \mathbb{R}^{n_1}, \mathbf{W}_k \in \mathbb{R}^{n_1 \times 2}, \vec{b}_k \in \mathbb{R}^{n_1}$  random initialization (e.g.,  $\mathcal{N}(0, 0.01)$ );
     $\Theta_k \leftarrow (\vec{a}_k, \mathbf{W}_k, \vec{b}_k)$ ;
end
 $\tilde{\Theta} \leftarrow (\Theta_1, \dots, \Theta_m)$ 

// Training Loop
best_loss  $\leftarrow \infty$ , wait  $\leftarrow 0$ 
for epoch = 1 to E do
    for each image  $\mathbf{f}_{\text{input}}^i \in \mathcal{F}_N$  do
        // Forward
        for k = 1 to m do
            Compute network outputs  $\mathbf{s}_\varepsilon[\Theta_k](\vec{x}) = \sum_{j=1}^{n_1} (\vec{a}_k)_j \sigma((\mathbf{W}_k)_j^T \vec{x} + (\vec{b}_k)_j)$ 
        end
        Compute region means  $c_i^\varepsilon(\tilde{\Theta}) = \frac{\int_{\Omega} \mathbf{f}(\vec{x}) \prod_{k=1}^m \sigma_\varepsilon(\iota_k \mathbf{s}_\varepsilon[\Theta_k](\vec{x})) d\vec{x}}{\int_{\Omega} \prod_{k=1}^m \sigma_\varepsilon(\iota_k \mathbf{s}_\varepsilon[\Theta_k](\vec{x})) d\vec{x}}$  for  $\iota \in \{-1, 1\}^m$ .
        // Loss
         $L \leftarrow E_{CV}^{\mathbf{f}, \varepsilon}(\{c_i^\varepsilon(\tilde{\Theta})\}_{\iota \in \{-1, 1\}^m}, \{\mathbf{s}_\varepsilon[\Theta_k]\}_{j=1}^m)$ 
        (+ optional supervised loss  $\mathcal{L}(\mathbf{f}_{\text{input}}^i - \mathbf{f}_{\text{target}}^i)$ )
        // Backward
        Compute the gradient  $\nabla_{\tilde{\Theta}} L$ 
        // Update
         $\tilde{\Theta} \leftarrow \text{Optimizer}(\tilde{\Theta}, \nabla_{\tilde{\Theta}} L)$ 
    end
    // Validation
    val_loss  $\leftarrow \frac{1}{|\mathcal{G}|} \sum_{\mathbf{g}^i \in \mathcal{G}} E_{CV}^{\mathbf{g}, \varepsilon}(\{c_i^\varepsilon(\tilde{\Theta})\}_{\iota \in \{-1, 1\}^m}, \{\mathbf{s}_\varepsilon[\Theta_k]\}_{j=1}^m)$ 
    if val_loss < best_loss then
        best_loss  $\leftarrow$  val_loss, wait  $\leftarrow 0$ 
         $\tilde{\Theta}_{\text{best}} \leftarrow \tilde{\Theta}$ 
    end
    else
        wait  $\leftarrow$  wait + 1
        if wait  $\geq P$  then
            break // Early stopping
        end
    end
end
end

return  $\tilde{\Theta}_{\text{best}} =: \bar{\Theta} = (\bar{\Theta}_1, \dots, \bar{\Theta}_m)$ 

// Testing
for new image g do
    Compute network outputs  $\mathbf{s}_\varepsilon[\bar{\Theta}_k]$ 
    Compute region means  $c_i^\varepsilon(\bar{\Theta})$ 
    Compute multiphase representation using  $\tilde{\Theta}_{\text{best}}$  and region means
     $\mathbf{m} = \sum_{\iota \in \{-1, 1\}^m} c_i^\varepsilon(\bar{\Theta}) \prod_{k=1}^m \sigma_\varepsilon(\iota_k \mathbf{s}_\varepsilon[\bar{\Theta}_k])$ 
end

```

Algorithm 2: Multiphase Parametrized Chan-Vese Segmentation with Mini-Batch SGD

Input: Image \mathbf{f} , number of phases $m \geq 1$, (optional) initial parameters $\{\Theta_k^0 = (\vec{a}_k^0, \mathbf{W}_k^0, \vec{b}_k^0)\}_{k=1}^m$, regularization constant $\mu > 0$, updating rate η , max iterations T , batch size B , smoothing parameter $\varepsilon > 0$, tolerance $\tau > 0$

Output: Optimized parameters $\{\Theta_k^*\}_{k=1}^m$, region means $\{c_i^*\}_{i \in \{-1,1\}^m}$, multiphase Chan-Vese function \mathbf{m}

// **Initialization:**

for $k = 1$ **to** m **do**

if Θ_k^0 *is not provided* **then**

$\vec{a}_k^0 \in \mathbb{R}^{n_1}$, $\mathbf{W}_k^0 \in \mathbb{R}^{n_1 \times 2}$, $\vec{b}_k^0 \in \mathbb{R}^{n_1}$ random initialization (e.g., $\mathcal{N}(0, 0.01)$)

$\Theta_k \leftarrow (\vec{a}_k, \mathbf{W}_k, \vec{b}_k)$;

end

else

$\Theta_k \leftarrow \Theta_k^0$;

end

 Compute $\mathbf{s}_\varepsilon[\Theta_k](\vec{x}) = \sum_{j=1}^{n_1} (\vec{a}_k)_j \sigma((\mathbf{W}_k)_j^T \vec{x} + (\vec{b}_k)_j)$

end

Calculate regions mean: $c_i^\varepsilon = \frac{\int_\Omega \mathbf{f}(\vec{x}) \prod_{k=1}^m \sigma_\varepsilon(\iota_k \mathbf{s}_\varepsilon[\Theta_k](\vec{x})) d\vec{x}}{\int_\Omega \prod_{k=1}^m \sigma_\varepsilon(\iota_k \mathbf{s}_\varepsilon[\Theta_k](\vec{x})) d\vec{x}}$ for $\iota \in \{-1, 1\}^m$.

// **Mini-batch SGD optimization**

for $t = 1$ **to** T **do**

$\mathcal{B} \leftarrow$ random batch of B pixels;

for $k = 1$ **to** m **do**

$\mathbf{g}_k \leftarrow \mathbf{0}$;

for $\vec{x} \in \mathcal{B}$ **do**

 Compute $\mathbf{s}_\varepsilon[\Theta_k](\vec{x}) = \sum_{j=1}^{n_1} (\vec{a}_k)_j \sigma((\mathbf{W}_k)_j^T \vec{x} + (\vec{b}_k)_j)$

$\mathbf{g}_k \leftarrow \mathbf{g}_k + \nabla_{\Theta_k} E_{CV}^{\mathbf{f}, \varepsilon}(\{c_i^\varepsilon\}_{i \in \{-1,1\}^m}, \{\mathbf{s}_\varepsilon[\Theta_k]\}_{j=1}^m)$

end

$\mathbf{g}_k \leftarrow \mathbf{g}_k / B$;

$\Theta_k \leftarrow \Theta_k - \eta \mathbf{g}_k$;

end

 Update region means $c_i^\varepsilon = \frac{\int_\Omega \mathbf{f}(\vec{x}) \prod_{k=1}^m \sigma_\varepsilon(\iota_k \mathbf{s}_\varepsilon[\Theta_k](\vec{x})) d\vec{x}}{\int_\Omega \prod_{k=1}^m \sigma_\varepsilon(\iota_k \mathbf{s}_\varepsilon[\Theta_k](\vec{x})) d\vec{x}}$ for $\iota \in \{-1, 1\}^m$.

 // **Early stopping**

if $\max_k \|\mathbf{g}_k\| < \tau$ **then**

break

end

end

// **Final segmentation**

$\mathbf{m} = \sum_{i \in \{-1,1\}^m} c_i \prod_{k=1}^m \sigma_\varepsilon(\iota_k \ell_k)$;

return $\{\Theta_k\}$, $\{c_i\}$, \mathbf{m} ;

4. NUMERICAL RESULTS

To verify our theoretical results, we run the parametrized Chan-Vese algorithm with $m = 4$ (allowing at most $2^4 = 16$ distinct segments) using both randomly initialized parameters and pre-trained parameters for initialization, and then compare the results.

Our algorithm (algorithm 2) requires an initialization of the level-set functions, which is computed from training samples. For training the initialization, we used algorithm 1. The datasets for training consist of 2000 images of size 50×50 pixels, each containing circles with variations in size and position. The datasets are split into training and validation sets using a 90–10 ratio. Each network, corresponding to a level-set function, is a linear neural network consisting of a single hidden layer with $8 \times 50 \times 50$ neurons. It uses the sigmoid activation function with $\varepsilon = 0.5$ and is trained using the AdamW optimizer with a learning rate of $3 \cdot 10^{-5}$ and a weight decay rate of 10^{-3} . The model is trained for 100 epochs, where each

epoch represents one full pass through the training dataset. The hyperparameters were chosen through iterative testing to best match the characteristics of our dataset and achieve stable training performance. For parametrized Chan-Vese functional optimization (algorithm 2), the regularization parameters are chosen as $\mu = 0.5, \nu = 0$. Smooth approximation of Heaviside and Dirac-delta functions are used with $\varepsilon = 0.5$. The gradient of the Chan-Vese functional with respect to the parameters is calculated using automatic differentiation (autograd), which relies on the analytic gradient calculation using the chain rule. The parameters are then optimized using AdamW.

Visualization results We evaluate performance qualitatively through visual inspection of the segmentation boundaries and compare the convergence behavior of the Chan-Vese functional across different conditions: using trained versus randomly initialized networks, varying ε values, and employing stochastic versus deterministic optimizers.

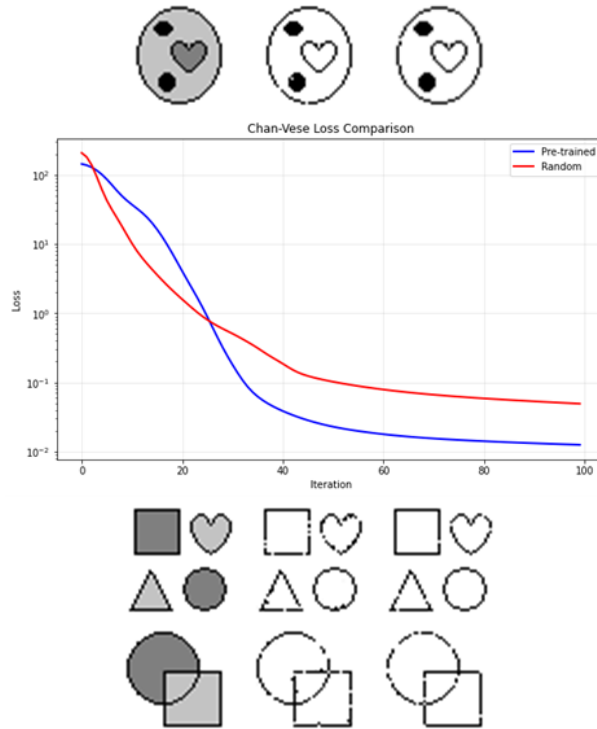


FIGURE 9. Input image \mathbf{f} to be segmented (left) and segmentation results of the parametrized Chan-Vese method after 50 iterations using randomized initialization (middle) and pre-trained initialization (right). The plot shows the corresponding parametrized Chan-Vese energy functional for the first input image.

From Figure 9, we observe that after 50 iterations, object boundaries are detected in both the pre-trained and randomly initialized cases. However, the boundaries obtained with random initialization are less clean and more irregular compared to those obtained with the pre-trained model. Some of these edge irregularities can be attributed to the inherent stochasticity of mini-batch optimizers. By operating on subsets of the data, these optimizers reduce memory and computational cost per iteration but introduce variability in the optimization path. This can result in isolated noisy pixels and minor differences in the final solution, even when starting from identical initializations and datasets, leading to slightly less consistent outcomes.

There is an inherent trade-off between precision and stability on one hand and speed and scalability on the other. Stochastic optimizers generally converge faster and require less memory per iteration compared to deterministic methods, which typically rely on full-gradient information. They are also less sensitive to initialization. In contrast, quasi-Newton methods, such as L-BFGS, can diverge depending on the starting point, making random initialization suboptimal. Overall, stochastic optimizers are faster, whereas L-BFGS with a good initialization tends to achieve higher precision. The choice of optimizer should be guided by the desired balance between computational efficiency and accuracy.

Furthermore, from the plot of the parametrized Chan-Vese energy functional, we observe that initially, the Chan-Vese energy value for the pre-trained initialization is lower than that of the randomized initialization, indicating that the pre-trained contours are initialized closer to the object. During the first 20 iterations, however, the randomly initialized parameters appear to converge faster than the pre-trained initialization. This occurs because the pre-trained contours start near the object, resulting in smaller gradients and slower early evolution, whereas randomly initialized contours, starting farther from the object, adjust coarse shapes more quickly during the initial steps. Notably, after approximately 22 iterations, the neural network prior parametrized version rapidly surpasses the random initialization, demonstrating that the prior improves both convergence speed and final performance.

We next examine the impact of the parameter ε , as visualized in Figure 10. From the Chan-Vese energy functional plot, the energy converges faster for $\varepsilon = 0.5$ than for $\varepsilon = 1$. Correspondingly, at early iterations (e.g., the 10th iteration), $\varepsilon = 0.5$ produces clearer results. However, after 50 iterations, the outputs for different ε values become approximately equivalent.

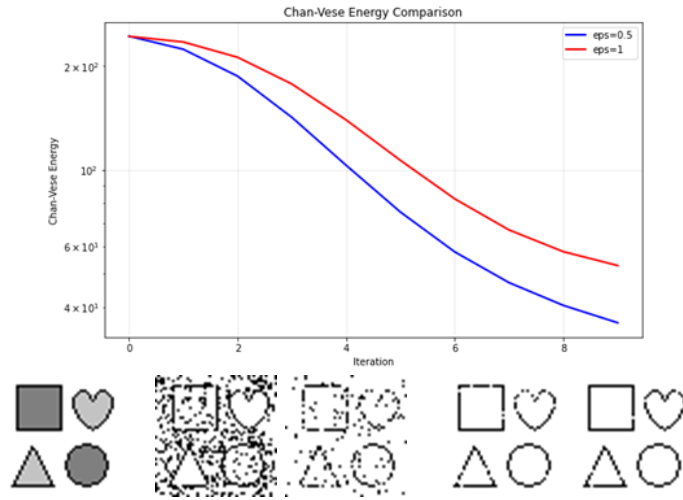


FIGURE 10. First row: Parametrized Chan-Vese energy functional for $\varepsilon = 0.5, 1$. Second row, from left to right: Input image and results of parametrized Chan-Vese algorithm after 10 iterations for $\varepsilon = 1, 0.5$, and after 50 iterations for $\varepsilon = 1, 0.5$.

Finally, the effect of the parameter μ in Equation 3.6 is illustrated in Figure 11. The energy functional converges similarly for the first 30 iterations, but differences become more noticeable after 40 iterations. Visual inspection indicates that $\mu = 0.1$ (the parameter in Equation 3.2) produces the clearest results.

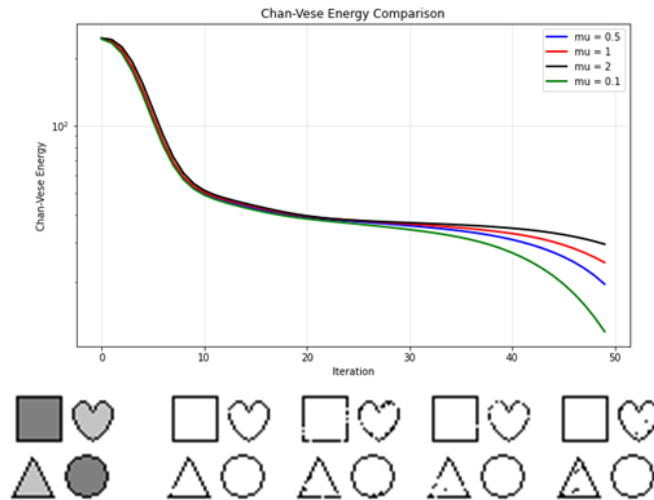


FIGURE 11. First row: Parametrized Chan-Vese energy functional for $\mu = 0.1, 0.5, 1, 2$. Second row, from left to right: Input image and results of parametrized Chan-Vese algorithm after 50 iterations for $\mu = 0.1, 0.5, 1, 2$.

5. APPROXIMATION RESULTS (APPENDIX)

Section 4 presented a reliable implementation of the numerical algorithms introduced in [algorithm 1](#) and [algorithm 2](#). In this section, we establish an approximation result showing that any construction involving the Heaviside activation function can be approximated by replacing it with a sigmoid function. Specifically, we quantify the difference between the original and smoothed problems introduced in [Section 3.3](#) and establish convergence as $\varepsilon \rightarrow 0$, thereby justifying the numerical implementation presented in [Section 3.4](#) and [Section 4](#). The result is summarized by the following approximation chain:

$$\mathbf{m}_\varepsilon \approx \mathbf{m} \approx \mathbf{t} \approx \mathbf{t}_\varepsilon.$$

The approximation procedure is summarized in four steps:

- (i) **Step 1 (Parametrization):** We reformulate the minimization problem by replacing the level-set function ℓ_k (defined in [Definition 3.2](#)) with a one-layer Heaviside neural network \mathbf{s} (defined in [Equation 2.3](#)). This parametrization is established in [Section 3](#).
- (ii) **Step 2 (Polygonal to general regions):** The parametrization initially yields segmentations consisting of polygonal regions, captured by the multi-phase level-set functions $\mathbf{m}_\mathbf{s}$ (see [Equation 3.8](#)). As shown in [Lemma 3.6](#), these functions can be represented pointwise in Ω by a weakly customized two-layer Heaviside network $\mathbf{t}_\mathbf{m}$. The main goal of this step is to extend this result to approximate arbitrary multi-phase functions \mathbf{m} whose regions have finite perimeter; that is, to establish $\mathbf{m} \approx \mathbf{t}$, as stated in [Theorem 5.2](#).
- (iii) **Step 3 (Heaviside to sigmoid):** We show that a one-layer Heaviside neural network \mathbf{s} can be approximated by a one-layer sigmoid neural network \mathbf{s}_ε . The validity of that is established in [Lemma 5.3](#). A similar result applies to two-layer networks.
- (iv) **Step 4 (Heaviside to sigmoid - multi-phase):** We extend the approximation to show that the smoothed multiphase level-set functions \mathbf{m}_ε (where σ is replaced by σ_ε) can be approximated by two-layer sigmoid neural networks \mathbf{t}_ε . This final result is proven in [Theorem 5.5](#).

In what follows, we provide rigorous proofs for Step 2 (see [Section 5.1](#)) and for Steps 3 and 4 (see [Section 5.2](#)).

5.1. Approximation by neural network parametrization with Heaviside activation.

We begin with Step 2, by establishing the approximation properties of the neural network parametrized method:

$$\mathbf{m} \approx \mathbf{t}_\mathbf{m} \text{ in } L^2(\Omega),$$

which rigorously justifies the approximation relation illustrated in [Figure 7](#).

This approximation result is proven in [Theorem 5.2](#), building on [Corollary 5.1](#) below. The latter states an $L^2(\Omega)$ approximation result for the parametrized multiphase level-set function $\mathbf{m}_\mathbf{s}$, where all regions S_i , as defined in [Equation 3.5](#), are polygons. [Corollary 5.1](#) is a direct extension of [Lemma 3.6](#) from [Section 3](#).

Corollary 5.1. *Every multiphase level-set function $\mathbf{m}_\mathbf{s}$, where all regions S_i are polygons (that is, regions bound by hyperplanes), can be represented by a two-layer neural network $\mathbf{t}_\mathbf{m} \in \mathbf{T}$ pointwise in Ω , in $L^1(\Omega)$ and $L^2(\Omega)$.*

From [Corollary 5.1](#), we derive the following quantitative approximation result for the multiphase level-set function \mathbf{m} , where the boundaries of the regions S_i are sets of finite perimeter.

Theorem 5.2. *Every multiphase level-set function \mathbf{m} , defined in [Equation 3.4](#), can be approximated in $L^2(\Omega)$ by a two-layer neural network $\mathbf{t}_\mathbf{m} \in \mathbf{T}$ (see [Equation 2.5](#)), defined in [Equation 2.6](#). In particular, for every $\delta > 0$, there exists a one-layer neural network $\mathbf{s}_k \in \mathbf{N}$ and a two-layer neural network $\mathbf{t}_\mathbf{m} \in \mathbf{T}$ such that*

$$\|\mathbf{m} - \mathbf{t}_\mathbf{m}\|_{L^2} \leq \delta.$$

The proof is a simple consequence of the fact that for a set of finite perimeter, the boundaries can be approximated by piecewise linear segments uniformly (see [3, Section 3.5]).

Theorem 5.2 shows the existence of a two-layer neural network \mathbf{t}_m that approximates the multiphase level-set function \mathbf{m} in $L^2(\Omega)$. However, the representation of such neural network approximations is not unique (see the next section for details). Hence, from now on, we use $\mathbf{m} \approx \mathbf{t}$ to refer to a general two-layer network instead of \mathbf{t}_m , which denotes the customized network defined in Equation 3.10. This completes Step 2; we now proceed to Step 3 and 4.

5.2. Neural network approximation using sigmoid activation.

In this section, we show that a sigmoid network can approximate a Heaviside network, and then extend this result to demonstrate that the smoothed multiphase level-set function can be approximated by two-layer sigmoid network:

$$\mathbf{m}_\varepsilon \approx \mathbf{t}_\varepsilon \text{ in } L^2(\Omega).$$

These results clarify how the choice of the smoothing parameter ε influences accuracy and stability (see Figure 10) and ensure that the smoothed formulation provides a consistent approximation of the original problem.

The main result of this section is stated in Theorem 5.5. It follows from Theorem 5.2 of the previous section, which establishes the relation $\mathbf{m} \approx \mathbf{t}$, together with the approximation of Heaviside networks by sigmoid networks established in Lemma 5.3 below. The proof of Lemma 5.3 relies on the properties of the sigmoid function stated in Lemma 3.7.

Lemma 5.3 (Existence). *Let $\Omega \subseteq \mathbb{R}^2$ be a bounded domain and let $n_1 \in \mathbb{N}$. For every one-layer neural network $\mathbf{s} \in \mathbb{N}$ with n_1 neurons and Heaviside activation σ , there exists a family $\{\mathbf{s}_\varepsilon \in \mathbb{N}_\varepsilon : \varepsilon > 0\}$ of one-layer neural networks with n_1 neurons and sigmoid activation such that*

$$\lim_{\varepsilon \rightarrow 0} \|\mathbf{s}_\varepsilon - \mathbf{s}\|_{L^2(\Omega)} = 0.$$

Lemma 5.3 can be proven with the dominated convergence theorem (see [6]). An analogous result holds for two-layer network, i.e., $\mathbf{t}_\varepsilon \approx \mathbf{t}$ in $L^2(\Omega)$.

A direct consequence of Lemma 5.3, together with the continuity of \mathbf{s}_ε with respect to its parameters, is the local approximability of \mathbf{s} : \mathbf{s} can be approximated by any \mathbf{s}_ε whose parameters are sufficiently close to those of \mathbf{s} . This demonstrates the non-uniqueness of sigmoid networks approximating a given Heaviside network.

Lemma 5.4 (Local approximation of \mathbf{s}). *Let $\Omega \subseteq \mathbb{R}^2$ be a bounded domain, and let $\varepsilon > 0$. Moreover, let $m \in \mathbb{N}$ be a fixed number of neurons and let $\mathbf{s}[\vec{a}, \mathbf{W}, \vec{b}] \in \mathbb{N}$ be a neural networks with Heaviside activation σ . Let $[\vec{a}_\varepsilon, \tilde{\mathbf{W}}_\varepsilon, \vec{b}_\varepsilon]$ satisfy*

$$d\left([\vec{a}_\varepsilon, \tilde{\mathbf{W}}_\varepsilon, \vec{b}_\varepsilon] - [\vec{a}, \mathbf{W}, \vec{b}]\right) < \varepsilon,$$

where d denotes the Euclidean distance, then it follows that

$$\lim_{\varepsilon \rightarrow 0} \left\| \mathbf{s}_\varepsilon[\vec{a}_\varepsilon, \tilde{\mathbf{W}}_\varepsilon, \vec{b}_\varepsilon] - \mathbf{s}[\vec{a}, \mathbf{W}, \vec{b}] \right\|_{L^2(\Omega)} = 0.$$

The proof follows from the triangle inequality and the Lipschitz continuity of σ_ε .

Finally, we can demonstrate the approximation properties of level-set functions via two-layer linear neural networks by extending the result of Lemma 5.3 together with Theorem 5.2.

Theorem 5.5 (Neural networks approximation of multiphase level-set function). *Let \mathbf{m}_ε be a multiphase level-set function as defined in Equation 3.4 where the Heaviside function σ is replaced by sigmoid function σ_ε . Then, for every $\varepsilon > 0$, there exists a two-layer network $\mathbf{t}_\varepsilon \in \mathbb{T}_\varepsilon$ (see Equation 2.5) with sigmoid activation such that*

$$\|\mathbf{m}_\varepsilon - \mathbf{t}_\varepsilon\|_{L^2(\Omega)} < \varepsilon.$$

Proof. Let $\varepsilon > 0$ be arbitrary but fixed. The estimate

$$\|\mathbf{m} - \mathbf{t}_\varepsilon\|_{L^2(\Omega)} < \frac{\varepsilon}{2}$$

follows from [Theorem 5.2](#) and [Lemma 5.3](#) for \mathbf{T} , combined by triangle inequality.

Since $\sigma_\varepsilon \rightarrow \sigma$ pointwise in \mathbb{R} , the smooth multiphase level-set function also converges pointwise to its standard version:

$$\lim_{\varepsilon \rightarrow 0} |\mathbf{m}_\varepsilon(\vec{x}) - \mathbf{m}(\vec{x})| = \lim_{\varepsilon \rightarrow 0} \left| \sum_{i \in \{-1,1\}^m} c_i \prod_{k=1}^m \sigma_\varepsilon(\iota_k \ell_k(\vec{x})) - \sum_{i \in \{-1,1\}^m} c_i \prod_{k=1}^m \sigma(\iota_k \ell_k(\vec{x})) \right| = 0 \quad \forall \vec{x} \in \Omega.$$

Both functions are uniformly bounded, so the dominated convergence theorem ensures convergence in $L^1(\Omega)$. Moreover, since $\|\mathbf{m}_\varepsilon - \mathbf{m}\|_{L^2}^2 \leq 2 \max\{\|\mathbf{m}_\varepsilon\|_\infty, \|\mathbf{m}\|_\infty\} \|\mathbf{m}_\varepsilon - \mathbf{m}\|_{L^2}$, convergence in $L^2(\Omega)$ follows as well. Thus, we obtain the estimate

$$\|\mathbf{m}_\varepsilon - \mathbf{m}\|_{L^2(\Omega)} < \frac{\varepsilon}{2}.$$

Combine the two estimates, we obtain the desired result. \square

[Theorem 5.5](#) concludes the approximation chain

$$\mathbf{t}_\varepsilon \approx \mathbf{t} \approx \mathbf{m} \approx \mathbf{m}_\varepsilon.$$

These approximation results also provide the foundation for the Γ -convergence considerations discussed below.

Remark 5.6 (Γ -convergence under certain regularity assumptions). In [Remark 3.8](#), we discussed the Γ -convergence of Chan-Vese smooth parametrized functional $\text{CV}_{\mathbf{f},\varepsilon}^{\text{LS}}$ to the original model $\text{CV}_{\mathbf{f}}^{\text{LS}}$, and the convergence of a neural network minimizers to a C^1 minimizer the limit functional. This result requires the existence of a sequence of one-layer sigmoid networks $\mathbf{s}_\varepsilon \in \mathbf{N}_\varepsilon$ converging to level-set function ℓ in $C^1(\bar{\Omega})$.

In this section, we have only established approximation in L^2 . The gap between L^2 and C^1 -convergence may cause difficulties, since the sigmoid converges to the discontinuous Heaviside function. This may lead to instability near edges or intersection points, as observed in [Figure 9](#).

Acknowledgements. This research was funded in whole, or in part, by the Austrian Science Fund (FWF) 10.55776/P34981 (OS) – New Inverse Problems of Super-Resolved Microscopy (NIPSUM), SFB 10.55776/F68 (OS) “Tomography Across the Scales”, project F6807-N36 (Tomography with Uncertainties), 10.55776/T1160 (CS) “Photoacoustic Tomography: Analysis and Numerics”, National Natural Science Foundation of China (Grant No. 41030040 (CS)), the Fundamental Research Funds for the Central Universities, Sun Yat-sen University (Grant No. 22qntd2901 (CS)). For open access purposes, the author has applied a CC BY public copyright license to any author-accepted manuscript version arising from this submission. The financial support by the Austrian Federal Ministry for Digital and Economic Affairs, the National Foundation for Research, Technology and Development and the Christian Doppler Research Association is gratefully acknowledged.

REFERENCES

- [1] R. A. Adams. “Sobolev Spaces”. Pure and Applied Mathematics 65. New York: Academic Press, 1975. ISBN: 9780080873817 (cited on page 3).
- [2] A. Aghasi, M. Kilmer, and E. L. Miller. “Parametric Level Set Methods for Inverse Problems”. In: *SIAM Journal on Imaging Sciences* 4.2 (2011), pp. 618–650. ISSN: 1936-4954. DOI: [10.1137/100800208](https://doi.org/10.1137/100800208) (cited on page 1).
- [3] L. Ambrosio, N. Fusco, and D. Pallara. “Functions of Bounded Variation and Free Discontinuity Problems”. 2000. DOI: [10.1093/oso/9780198502456.001.0001](https://doi.org/10.1093/oso/9780198502456.001.0001) (cited on page 17).
- [4] T. F. Chan and L. A. Vese. “Active contours without edges”. In: *IEEE Transactions on Image Processing* 10.2 (2001), pp. 266–277. ISSN: 1057-7149. DOI: [10.1109/83.902291](https://doi.org/10.1109/83.902291) (cited on pages 1, 6, 7).
- [5] G. Dal Maso. “An Introduction to Γ -Convergence”. 1993. DOI: [10.1007/978-1-4612-0327-8](https://doi.org/10.1007/978-1-4612-0327-8) (cited on page 11).
- [6] L. C. Evans and R. F. Gariepy. “Measure theory and fine properties of functions”. Revised. Textbooks in Mathematics. Boca Raton, FL: CRC Press, 2015. xiv+299. ISBN: 978-1-4822-4238-6 (cited on page 17).
- [7] R. Feichtinger, M. Fuchs, B. Jüttler, O. Scherzer, and H. Yang. “Dual evolution of planar parametric spline curves and T-spline level sets”. In: *Computer Aided Design* 40.1 (2008), pp. 13–24. ISSN: 0010-4485. DOI: [10.1016/j.cad.2007.08.003](https://doi.org/10.1016/j.cad.2007.08.003) (cited on page 1).
- [8] M. Fuchs, B. Jüttler, O. Scherzer, and H. Yang. “Combined evolution of level sets and B-spline curves for imaging”. In: *Computing and Visualization in Science* 12.6 (2009), pp. 287–295. ISSN: 1432-9360. DOI: [10.1007/s00791-008-0110-4](https://doi.org/10.1007/s00791-008-0110-4) (cited on page 1).
- [9] J. M. Morel and S. Solimini. “The Piecewise Constant Mumford and Shah Model: Mathematical Analysis”. In: *Variational Methods in Image Segmentation*. 1995, pp. 46–62. DOI: [10.1007/978-1-4684-0567-5_5](https://doi.org/10.1007/978-1-4684-0567-5_5) (cited on pages 1, 7, 11).
- [10] D. Mumford and J. Shah. “Optimal approximations by piecewise smooth functions and associated variational problems”. In: *Communications on Pure and Applied Mathematics* 42.5 (1989), pp. 577–685. ISSN: 0010-3640. DOI: [10.1002/cpa.3160420503](https://doi.org/10.1002/cpa.3160420503) (cited on page 1).
- [11] S. Osher and J. A. Sethian. “Fronts propagating with curvature-dependent speed: Algorithms based on Hamilton-Jacobi formulations”. In: *Journal of Computational Physics* 79.1 (1988), pp. 12–49. ISSN: 0021-9991. DOI: [10.1016/0021-9991\(88\)90002-2](https://doi.org/10.1016/0021-9991(88)90002-2) (cited on page 1).
- [12] E. Ozsar, M. Kilmer, E. de Sturler, A. K. Saibaba, and E. Miller. “Parametric level-sets enhanced to improve reconstruction (PaLEnTIR)”. In: *Inverse Problems* 41.2 (2025), p. 025004. ISSN: 0266-5611. DOI: [10.1088/1361-6420/ada798](https://doi.org/10.1088/1361-6420/ada798) (cited on page 1).
- [13] J. Steiner. “Einige Gesetze über die Theilung der Ebene und des Raumes.” In: *Journal für die reine und angewandte Mathematik* 1 (1826), pp. 349–364 (cited on page 6).
- [14] L. A. Vese and T. F. Chan. In: *International Journal of Computer Vision* 50.3 (2002), pp. 271–293. ISSN: 0920-5691. DOI: [10.1023/a:1020874308076](https://doi.org/10.1023/a:1020874308076) (cited on pages 1, 6, 7, 9).

-
- [15] H. Yang, M. Fuchs, B. Jüttler, and O. Scherzer. “Evolution of T-spline Level Sets with Distance Field Constraints for Geometry Reconstruction and Image Segmentation”. In: *Proceedings of the IEEE International Conference on Shape Modeling and Applications 2006 (SMI06)*. Matsushima, Japan: IEEE Computer Society, 2006, p. 37. ISBN: 0-7695-2591-1. DOI: [10.1109/smi.2006.12](https://doi.org/10.1109/smi.2006.12) (cited on page 1).